Atomic and electronic structures of $CaCO_3$ surfaces

Toru Akiyama,* Kohji Nakamura, and Tomonori Ito
Department of Physics Engineering, Mie University, 1577 Kurima-Machiya, Tsu 514-8507, Japan
(Received 4 May 2011; revised manuscript received 6 July 2011; published 25 August 2011)

The atomic structures and electronic states of $CaCO_3$ surfaces in calcite and aragonite polymorph are theoretically investigated by performing electronic structure calculations within the density-functional theory. The calculated surface energies demonstrate that in both calcite and aragonite structures the surfaces, containing the same number of Ca atoms as $CaCO_3$ groups around the top layer, are stabilized irrespective of the chemical potentials of constituting elements. The analysis of the electronic structures clarifies that the transfer of electrons between $4s$ orbitals of Ca atoms into $2p$ orbitals of O atoms, which are located near the surface, is crucial for the stabilization. Furthermore, we find the surface states caused by $2p$ orbitals of the O atoms in triangular CO_3^{2-} located at the top or second layer appear above the valence band maximum of bulk $CaCO_3$, leading to the reduction of C-O bonds of carbonate groups near the surfaces. The emergence of these surface states implies a possibility to identify the atomic structures by spectroscopic measurements.

DOI: 10.1103/PhysRevB.84.085428 PACS number(s): 68.35.Md, 68.35.bt, 73.20.At

I. INTRODUCTION

Calcium carbonate ($CaCO_3$) is one of the most abundant minerals and continues to attract much interest both from scientific and technological viewpoints. $CaCO_3$ has a potential for the application of surface interactions with heavy metals,[1] industrial water treatment,[2] and energy storage.[3] Among several polymorphs of calcium carbonate, calcite and aragonite are the most important crystalline forms. The most stable form at room temperature and atmospheric pressure is calcite, which has a rhombohedral crystal structure with space group $R\bar{3}c$. Aragonite, which is composed by biogenic environments, has an orthorhombic crystal structure with space group $Pmcn$ and is metastable. These $CaCO_3$ polymorphs have been the subject of extensive experimental and theoretical research.

Knowledge of $CaCO_3$ surface also facilitate a more rigorous understanding of dynamic processes during the growth of $CaCO_3$ and is therefore important for a wide range of applications. The structure of calcite surface has been studied by a variety of experimental methods. Hence, the nucleation under compressed Langmuir monolayers of calcite has been observed by the scanning electron microscopy (SEM).[4] The scanning force microscopy observation have examined the optical quality of calcite cleavage $\{10\bar{1}4\}$ surface and revealed the formation of hillocks and holes on terraces and cleavage steps.[5] The cleavage $\{10\bar{1}4\}$ surface has also been investigated by the atomic force microscopy (AFM) and their atomic scale images are interpreted in terms of the top-lying surface oxygen atoms.[6–9] X-ray diffraction have been used to measure the lattice locations of atoms within and at the surface of $\{10\bar{1}4\}$ plane.[10,11] Moreover, structure and bonding environments at the calcite surface have been examined by x-ray photoelectron spectroscopy and low-energy electron diffraction (LEED).[12] Although experimental studies for aragonite surfaces are relatively poor compared with those of calcite surfaces, the structure and nucleation of aragonite have been observed by the SEM[4,13,14] and transmission-electron microscopy.[4]

In order to clarify the structures and stability of $CaCO_3$ surfaces, there have been performed several theoretical calculations. As for calcite $\{10\bar{1}4\}$ plane, which is experimentally dominant surface, the surface energy containing both Ca ions and CO_3 groups obtained by empirical interatomic potentials[15–18] and density-functional theory (DFT) calculations[19,20] has the lowest value among various orientations. Both empirical interatomic potentials and DFT calculations have also been performed to calculate the surface energy of calcite $\{01\bar{1}2\}$ surface with different surface termination and clarified that the surface terminated by 0.5 coverage of Ca ($\theta_{Ca} = 0.5$) is the most stable.[17,21] However, the relative stability among different surface termination and effects of the growth conditions on the stability is still unclear. Furthermore, little is known about electronic structures of these surfaces. In the case of aragonite surfaces, there are few theoretical calculations for their atomic and electronic structures. Although surface energies of experimentally observed planes, such as {010}, {001}, and {110} surfaces,[4,13,14,22,23] have been calculated using empirical interatomic potential,[15] the energetics among the surfaces with different termination, detailed atomic arrangements, and their electronic structures are unknown at the present stage.

In this paper, we systematically investigate atomic structures and electronic states of various $CaCO_3$ surfaces using the electronic structure calculations within the density-functional theory. The calculated results provide detailed atomic structures, surface stoichiometries, the stability among various surface structures as a function of chemical potentials of constituting elements, and the electronic structures. Effects of charge transfer between Ca atoms and carbonate groups on the stability of $CaCO_3$ surfaces are also discussed in terms of their electronic structures. In Sec. II, we describe our methodology, and Sec. III contains the main results and discussion for atomic and electronic structures of calcite and aragonite surfaces. Section IV summarizes our findings.

II. COMPUTATIONAL DETAILS

Total energy calculations are performed within the framework of DFT[24,25] with the generalized gradient approximation.[26] We employ ultrasoft pseudopotentials to simulate nuclei and core electrons.[27] To generate pseudopotentials, $2s$ and $2p$ electrons in O and N atoms are treated as valence orbital, and $3s$, $3p$, and $4s$ orbitals of

TABLE I. Calculated lattice parameters and energy gap E_g of $CaCO_3$ calcite and aragonite in the bulk phase, along with the corresponding experimental values.[31–33] Note that calcite has a rhombohedral crystal structure with space group $R\bar{3}c$, which satisfies $a = b$. To our knowledge, there is no experimental data available for the energy gap of aragonite.

	Polymorph	a (Å)	b (Å)	c (Å)	E_g (eV)
Calc.	calcite	5.039	5.039	17.456	5.06
	aragonite	5.112	8.230	5.915	4.24
Expt.	calcite[a]	4.991	4.991	17.062	6.0 ± 0.35
	aragonite[b]	4.962	7.969	5.743	

[a]References 31 and 32.
[b]Reference 33.

Ca atom are regarded as valence electrons. The conjugate gradient technique[28–30] is utilized for both electronic structure calculation and geometry optimization. In the optimized geometries, the remaining forces acting on the atoms are less than 5.0×10^{-3} Ry/Å. The valence wave functions are expanded by the plane-wave basis set with a cutoff energy of 25 Ry. Prior to the calculations of $CaCO_3$ surfaces, we examine structural and electronic properties of $CaCO_3$ in the bulk phase. Table I shows the calculated lattice parameters and energy gap of calcite and aragonite structures, along with those in the experiments.[31–33] The differences between the calculated lattice parameters and corresponding experimental values are within +2.2 and +3.3% for calcite and aragonite, respectively, which are comparable to those in the previous calculations.[34–38] The calculated C-O bond lengths are ranging 1.30−1.31 Å, which are almost identical to those obtained in the previous calculations.[35,38] The calculated energy gaps of calcite and aragonite (5.11 and 4.24 eV, respectively) agree well with those obtained in the previous studies.[34,35,38] The calculated energy gap of calcite is found to be 16% smaller than that in the experiment (6.0 eV),[32] which is a typical DFT underestimation of the experimental value.

$CaCO_3$ surfaces are simulated by repeating slab models with the ∼9 Å vacuum region which is enough to obtain accurate surface energies. The surfaces are constructed by five bilayers and four trilayers for calcite and aragonite surfaces, respectively.[39] All the atoms excepting those belonging to central bilayer and trilayer in the slab of calcite and aragonite, respectively, are fully relaxed. The calculated lattice parameters shown in Table I are used to generate the unit cells parallel to the surfaces. We use eight k points sampling for the 1×1 surface unit, which provides sufficient accuracy in the total energy. Both sides of the slab are identical and inversion symmetry is maintained. The macroscopic dipole is removed and the neutrality of the simulation cell is ensured by two equivalent surfaces on the opposite sides of the slab.

The relative stability among various surface structures is evaluated by the surface energy. The surface energy E_{surf} is the energy cost to form the surface, which is defined as

$$E_{\mathrm{surf}} = E_{\mathrm{tot}} - n_{\mathrm{Ca}}\mu_{\mathrm{Ca}} - n_{\mathrm{C}}\mu_{\mathrm{C}} - n_{\mathrm{O}}\mu_{\mathrm{O}}, \quad (1)$$

where E_{tot} is the total energy in the slab, μ_α is the chemical of potential of α species, and n_α is the number of α atoms. Here, we assume that the surface is in equilibrium with bulk $CaCO_3$ expressed as

$$\mu^{\mathrm{bulk}}_{\mathrm{CaCO_3}} = \mu_{\mathrm{Ca}} + \mu_{\mathrm{C}} + 3\mu_{\mathrm{O}}, \quad (2)$$

where $\mu^{\mathrm{bulk}}_{\mathrm{CaCO_3}}$ is the chemical potential of bulk $CaCO_3$. Each CO_3 group can be assumed as a rigid unit and the reconstruction can be formed by Ca atoms and CO_3 groups, leading to the relationship $3n_{\mathrm{C}} = n_{\mathrm{O}}$. Owing to these assumptions, the surface energy E_{surf} is calculated as a function of μ_{Ca} written as

$$E_{\mathrm{surf}} = E_{\mathrm{tot}} - (n_{\mathrm{Ca}} - n_{\mathrm{C}})\mu_{\mathrm{Ca}} - n_{\mathrm{C}}\mu^{\mathrm{bulk}}_{\mathrm{CaCO_3}}. \quad (3)$$

The chemical potential of Ca varies depending on experimental environments, so that the surface energy can be varied by the environments. Moreover, there are upper and lower limits in the chemical potential. The upper limit of μ_{Ca} is the chemical potential of bulk Ca ($\mu^{\mathrm{bulk}}_{\mathrm{Ca}}$), since μ_{Ca} larger than this value results in the formation of bulk Ca, which corresponds to the segregation of Ca metal from $CaCO_3$. According to the relationship expressed by Eq. (2), the lower limit of μ_{Ca} corresponds to the upper limits of μ_{C} and μ_{O}. These upper limits can be obtained by considering the vaporization as CO_2 and O_2 molecules. Therefore μ_{Ca} can vary in the thermodynamically allowed range $\mu^{\mathrm{bulk}}_{\mathrm{Ca}} + \Delta H_f \leqslant \mu_{\mathrm{Ca}} \leqslant \mu^{\mathrm{bulk}}_{\mathrm{Ca}}$. The heat of formation ΔH_f is defined as

$$\Delta H_f = E^{\mathrm{bulk}}_{\mathrm{CaCO_3}} - E_{\mathrm{CO_2}} - \tfrac{1}{2}E_{\mathrm{O_2}} - E^{\mathrm{bulk}}_{\mathrm{Ca}}, \quad (4)$$

where $E^{\mathrm{bulk}}_{\mathrm{CaCO_3}}$, $E_{\mathrm{CO_2}}$, $E_{\mathrm{O_2}}$, and $E^{\mathrm{bulk}}_{\mathrm{Ca}}$ are the total energies of $CaCO_3$ in the bulk phase, a CO_2 molecule, an O_2 molecule, and Ca in the bulk phase (face-centered-cubic structure), each of which is calculated independently. The calculated values of ΔH_f for calcite and aragonite in this study are −6.93 and −6.90 eV (-11.10×10^{-19} and -11.05×10^{-19} J), respectively.

III. RESULTS AND DISCUSSION

A. Calcite {10$\bar{1}$4} surface

The {10$\bar{1}$4} planes is frequently observed and dominate the morphology of calcite crystal. Each layer in the 1×1 unit cell is constructed of two Ca atoms and two CO_3 groups satisfying $\theta_{\mathrm{Ca}} = \theta_{\mathrm{CO_3}} = 1$. Due to this layer unit, we can consider the surface with different termination of $CaCO_3$ satisfying $(\theta_{\mathrm{Ca}},\theta_{\mathrm{CO_3}}) = (0,1), (1,0), (0.5,1), (1,0.5)$, and (0.5, 0.5) by removing Ca atoms or CO_3 groups in the 1×1 lateral periodicity. The surface energies of five distinctive structures with the 1×1 lateral periodicity are calculated in this study. In order to find the stability of the 2×1 reconstruction, which has been observed in the AFM[7,9] and LEED,[12] we perform the calculations for the 2×1 reconstruction caused by height deviation of the protruding O atoms in CO_3 groups along the [0100] direction. The calculations for the $c(2 \times 2)$ surfaces with $(\theta_{\mathrm{Ca}},\theta_{\mathrm{CO_3}}) = (0,1)$ and $(1,0)$ are also performed to clarify effects of two-dimensional symmetry on the stability of {10$\bar{1}$4} surface. Figure 1 shows the calculated surface energies of calcite {10$\bar{1}$4} surface as a function of Ca chemical potential. The surfaces with $\theta_{\mathrm{Ca}} = \theta_{\mathrm{CO_3}} = 1$ have low surface energies for the possible range of Ca chemical potential. The surface energies of $\theta_{\mathrm{Ca}} = \theta_{\mathrm{CO_3}} = 1$ with the 1×1 and

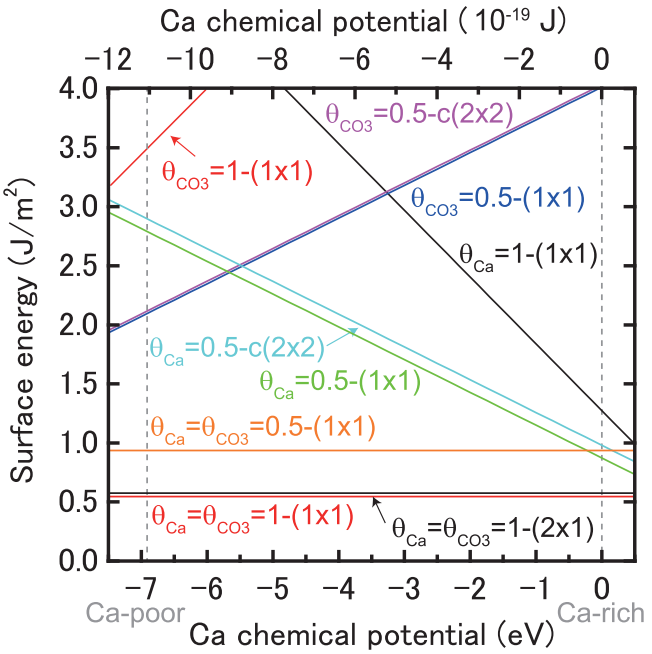

FIG. 1. (Color online) Calculated surface energy E_{surf} (in J/m^2) of calcite $\{10\bar{1}4\}$ surface as a function of Ca chemical potential μ_{Ca}. The left and right (vertical) dashed lines correspond to Ca-poor (lower limit of μ_{Ca}) and Ca-rich (upper limit of μ_{Ca}) environments, respectively.

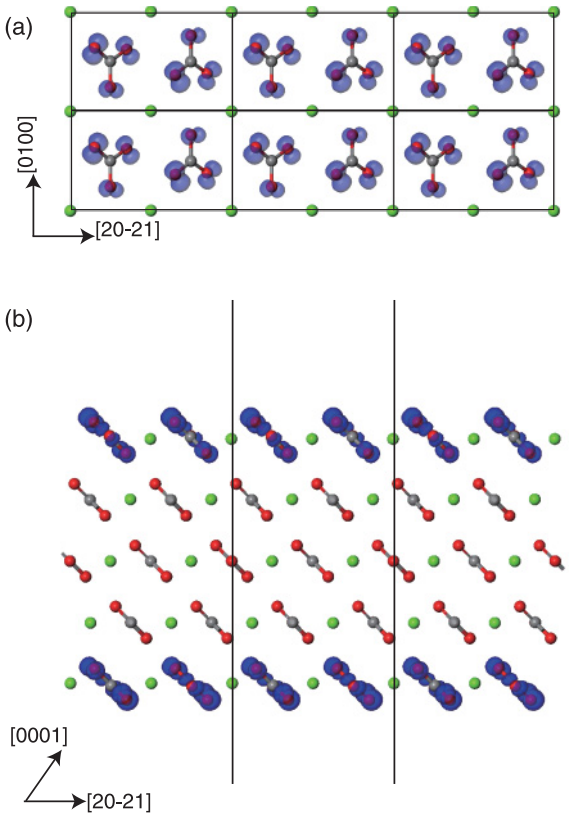

FIG. 2. (Color online) (a) Top and (b) side views of the optimized geometry of the stable calcite $\{10\bar{1}4\}$-(1 × 1) surface with $\theta_{Ca} = \theta_{CO_3} = 1$. Green, gray, and red circles represent calcium, carbon, and oxygen atoms, respectively. The unit cell of slab is enclosed by solid lines. Isosurface of squared wave function of the occupied surface state (0.005 electron/Å^3) at Γ point, which is located at 0.4 eV above the valence band maximum of bulk $CaCO_3$, is also shown. Top view shows only outermost Ca atoms and CO_3 groups, and the wave function around these atoms.

2 × 1 reconstructions (0.51 and 0.52 J/m^2, respectively) are irrespective of Ca chemical potential and agree well with those obtained in the previous calculations.[15–20] The surface energy of other structure is higher than that for $\theta_{Ca} = \theta_{CO_3} = 1$ with the 1 × 1 reconstruction by more than 0.26 J/m^2, even though Ca-rich ($\theta_{Ca} = 0.5$) and CO_3-rich ($\theta_{CO_3} = 0.5$) surfaces have low energies under Ca-rich and Ca-poor conditions, respectively. The calculated results thus suggest that the $\{10\bar{1}4\}$ plane experimentally observed corresponds to the surface with $\theta_{Ca} = \theta_{CO_3} = 1$. The surface energy of $\theta_{Ca} = \theta_{CO_3} = 1$ with the 2 × 1 reconstruction is found to be higher than that with the 1 × 1 reconstruction by only 0.01 J/m^2. The formation of cleavage steps which occasionally appear on the $\{10\bar{1}4\}$ surface could change the relative stability between the 1 × 1 and 2 × 1 reconstructions. It should be noted that the energies of the 1 × 1 surface with $\theta_{Ca} = 0.5$ and $\theta_{CO_3} = 0.5$ are lower than their counterparts with the $c(2 \times 2)$ periodicity, but the energy differences are small (∼0.11 J/m^2). We thus expect that the effects of two-dimensional symmetry on the surface energy is negligible on the $\{10\bar{1}4\}$ plane.

Figure 2 depicts the optimized geometry of the stable $\{10\bar{1}4\}$-(1 × 1) surface with $\theta_{Ca} = \theta_{CO_3} = 1$ obtained in the present calculation. The overall features of its atomic configuration are substantially the same as that in the previous calculations.[15] Even though there are two differently oriented CO_3 groups at the top layer, the outermost atoms consist of oxygen atoms of carbonate groups, consistent with the AFM observations.[6–9] We find that the spacing between the first and second layer (3.15 Å) is only ∼3% reduced compared to the layer spacing in the bulk calcite. Accordingly, the energy gain caused by the atomic relaxation (0.08 J/m^2) is small compared to the surface energy itself. It is thus concluded that the atomic relaxation in the lateral plane is minor contribution to the stability. Another prominent feature of the stable surface obtained by the calculations is the C-O bond length at the top layer. The outermost C-O bond lengths of CO_3 groups in the top layer (1.27 Å) are shorter than those of bulk calcite, whereas the other bond lengths of top layer CO_3 groups (1.30–1.31 Å) have similar values to those in the bulk region. This implies that there exist surface states that result in the reduction of the C-O bond lengths at the top layer.

Figure 3 shows calculated energy band of the stable surface. The valence bands of bulk $CaCO_3$ near the Fermi energy have a character of oxygen 2p orbitals, while the conduction bands of bulk $CaCO_3$ near the Fermi energy consist of carbon 2p orbitals and those above 6 eV are originating from Ca 4s orbitals. In the case of the stable surface on $\{10\bar{1}4\}$ plane, the energy band clearly shows a semiconducting character. On the other hands, the energy bands of the other surfaces exhibit metallic nature in which the highest occupied and lowest unoccupied states correspond to 2p orbitals of C and O atoms for Ca-rich and CO_3-rich (Ca-poor) surfaces, respectively. This implies that at the top layer of the stable surface 4s electrons of the Ca atoms are completely transferred into 2p orbitals of the O atoms of CO_3 groups. Therefore the stabilization of

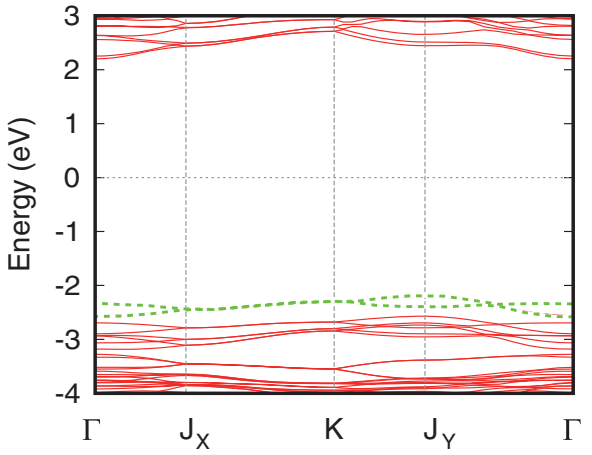

FIG. 3. (Color online) Energy band structures of the stable calcite $\{10\bar{1}4\}$-(1×1) surface with $\theta_{Ca} = \theta_{CO_3} = 1$. The occupied surface state is represented by green (dashed) lines. The Fermi energy is set to the origin of energy.

the surface with $\theta_{Ca} = \theta_{CO_3} = 1$ can be interpreted in terms of the electron counting model,[40] which successfully explains the stability of semiconductor surfaces. Another important feature of the energy band is the emergence of surface states. We find that the completely occupied surface states emphasized by green (dashed) lines in Fig. 3 are located above the valence band maximum of bulk $CaCO_3$. Our analysis of corresponding Kohn-Sham orbitals shown in Fig. 2 clearly shows that these states possess the character of $2p$ orbitals of the O atoms located at the top layer. These surface states are lifted up from corresponding valence bands by ~0.4 eV, since no Ca atoms, which are positively charged, are coordinated above the top layer. We expect that these surface states can be identified by spectroscopic measurements.

B. Calcite $\{01\bar{1}2\}$ surface

The $\{01\bar{1}2\}$ planes is also observed and dominate the morphology of calcite crystal. The ideal $\{01\bar{1}2\}$ plane composed of alternating layers of Ca ions and CO_3 groups each of which is constructed of two Ca atoms and CO_3 groups, respectively. Therefore depending on the coverage of Ca and CO_3, there are four distinctive ways of surface termination of $CaCO_3$ in the 1×1 lateral periodicity, and these surface terminations can be constructed by removing or attaching Ca atoms and CO_3 groups with each other. Moreover, there are different ways of removal of surface atoms, which form the $c(2 \times 2)$ lateral periodicity. In order to find effects of two-dimensional symmetry on the stability of surface, we furthermore perform calculations for the $c(2 \times 2)$ surfaces with $\theta_{Ca} = 0.5$ and $\theta_{CO_3} = 0.5$. The calculated surface energies of calcite $\{01\bar{1}2\}$ surface as a function of Ca chemical potential shown in Fig. 4 indicate that the surface energies for $\theta_{CO_3} = 0.5$ have lower values irrespective of Ca chemical potentials. In particular, the energy of the 1×1 surface satisfying $\theta_{CO_3} = 0.5$ has the lowest surface energy over the entire range of Ca chemical potential. The calculated surface energy (0.72 J/m^2) agrees with the value in previous first-principles calculation.[21] The surface energy of the other structure is higher than that

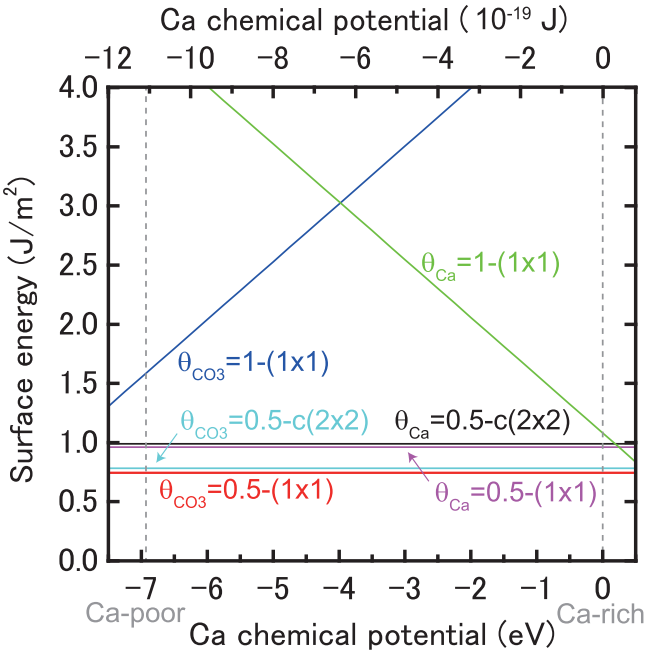

FIG. 4. (Color online) Calculated surface energy E_{surf} (in J/m^2) of calcite $\{01\bar{1}2\}$ surface as a function of Ca chemical potential μ_{Ca}. The notation is the same as in Fig. 1.

for $\theta_{CO_3} = 0.5$ by more than 0.19 J/m^2. Therefore it is likely that the $\{01\bar{1}2\}$ plane experimentally observed corresponds to the surface with $\theta_{CO_3} = 0.5$. Similar to the case of $\{10\bar{1}4\}$ surface, the energy difference between the 1×1 and $c(2 \times 2)$ surfaces are found to be small (~0.02 J/m^2). The effects of two-dimensional symmetry on the surface energy is thus expected to be negligible on the $\{01\bar{1}2\}$ plane.

Figure 5 depicts the optimized geometry of the stable $\{01\bar{1}2\}$-(1×1) surface with $\theta_{CO_3} = 0.5$ obtained in the present calculation. One of prominent features of the surface relaxation different from that on the $\{10\bar{1}4\}$ surface is the contraction of the spacing between the top layer CO_3 groups and the second Ca layer. The space is found to be reduced by 35% compared to that in the bulk phase. In particular, the CO_3 groups at the top layer are rotated and their triangulars are aligned almost parallel to the $\{01\bar{1}2\}$ plane. Accordingly, the contribution of surface relaxation on the surface energy (0.39 J/m^2) is of significance on the $\{01\bar{1}2\}$ surface. These results are consistent with those in the previous calculations.[21] Similar to the $\{10\bar{1}4\}$ surface, we find that the outmost C-O bond lengths of CO_3 groups in the top layer (1.28 Å) is shorter than those in the bulk region. This also implies that the presence of surface states that result in the reduction of the C-O bond lengths at the top layer.

Indeed, we find the surface states caused by the CO_3 groups at the top layer as shown in Fig. 6. The energy band of the stable $\{01\bar{1}2\}$ surface with $\theta_{CO_3} = 0.5$ shown in Fig. 6 clearly shows a semiconducting electronic structure similar to that of the stable $\{10\bar{1}4\}$ surface. This is originating from the transfer of $4s$ electrons of the Ca atoms in the second layer into $2s$ orbitals of the O atoms in CO_3 group at the top layer. The completely occupied surface states emphasized by green (dashed) lines in Fig. 6 are found to be located ~0.8 eV above the valence band maximum of bulk $CaCO_3$, and the wave-function distribution

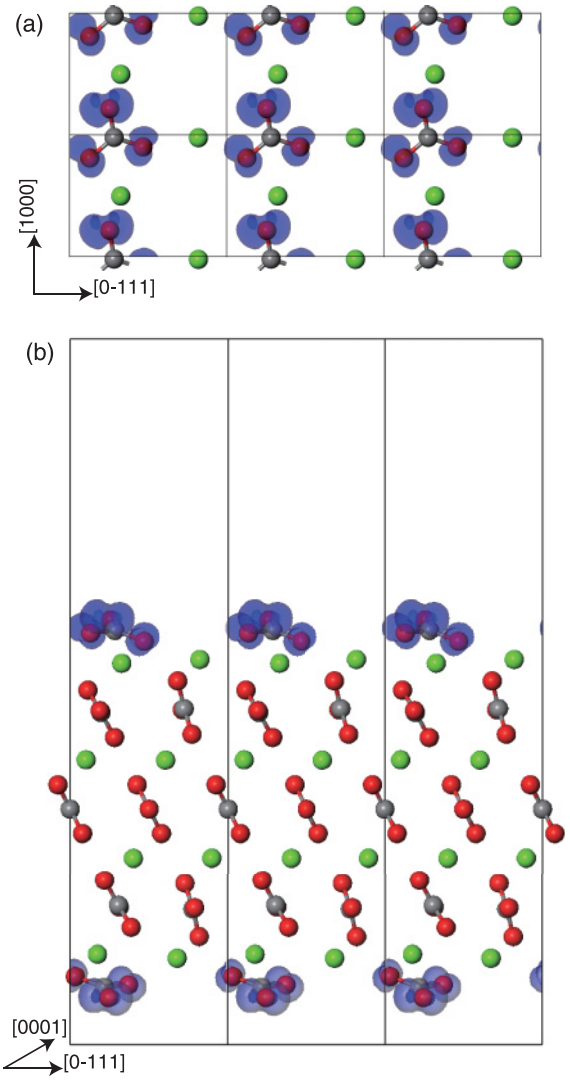

FIG. 5. (Color online) (a) Top and (b) side views of the optimized geometry of the stable calcite $\{01\bar{1}2\}$-(1×1) surface with $\theta_{CO_3} = 0.5$. The notation is the same as in Fig. 2. Isosurface of squared wave function for the occupied surface state (0.005 electron/Å^3) at Γ point which is located at 0.8 eV above the valence band maximum of bulk $CaCO_3$, is also shown.

of corresponding Kohn-Sham orbitals shown in Fig. 5 clearly indicates that these states possess the character of $2p$ orbitals of the O atoms located at the top layer. Due to the absence of positively charged Ca ions above the top layer, these surface states are lifted up from the corresponding valence bands.

C. Aragonite {001} surface

For aragonite {001} surface,[41] there is a layer unit consisting of three atomic layers along the [001] direction. Therefore, the layer unit in the 1×1 lateral unit of the {001} surface consists of two CO_3 layers each of which is constructed of one CO_3 group, and a Ca layer constructed of two Ca atoms. Due to this layer unit, there are three distinctive ways of termination of $CaCO_3$ in which the coverage of these surfaces satisfies either $\theta_{Ca} = 1$, $\theta_{CO_3} = 0.5$, or $\theta_{CO_3} = 1$. By removing one Ca atom in the in the 1×1 lateral unit at $\theta_{Ca} = 1$, we can

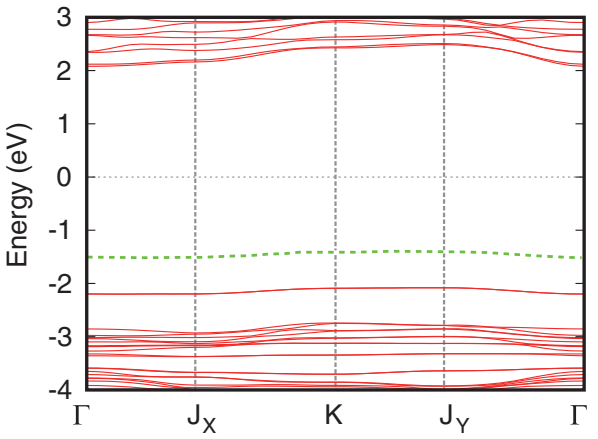

FIG. 6. (Color online) Energy band structures of the stable calcite $\{01\bar{1}2\}$-(1×1) surface with $\theta_{CO_3} = 0.5$. The notation is the same as in Fig. 3.

construct both 1×1 and $c(2 \times 2)$ surfaces with $\theta_{Ca} = 0.5$. We thus consider five distinctive structures on the {001} surface in the present study. Figure 7 shows the calculated surface energies of aragonite {001} surface as a function of Ca chemical potential. The surface satisfying $\theta_{CO_3} = 0.5$ has the lowest surface energy for the possible range of Ca chemical potential. However, the calculated surface energy of 0.57 J/m^2 is lower than those in previous calculation (0.85 J/m^2).[15] The difference between present DFT calculation and the empirical potential calculation might be due to the effect of dipole moments, which are locally formed between CO_3^{2-} in the top layer and Ca^{2+} in the second layer. The surface energy of other structure is higher than that for $\theta_{CO_3} = 0.5$ by more than 0.16 J/m^2, even though the surfaces satisfying $\theta_{Ca} = 1$

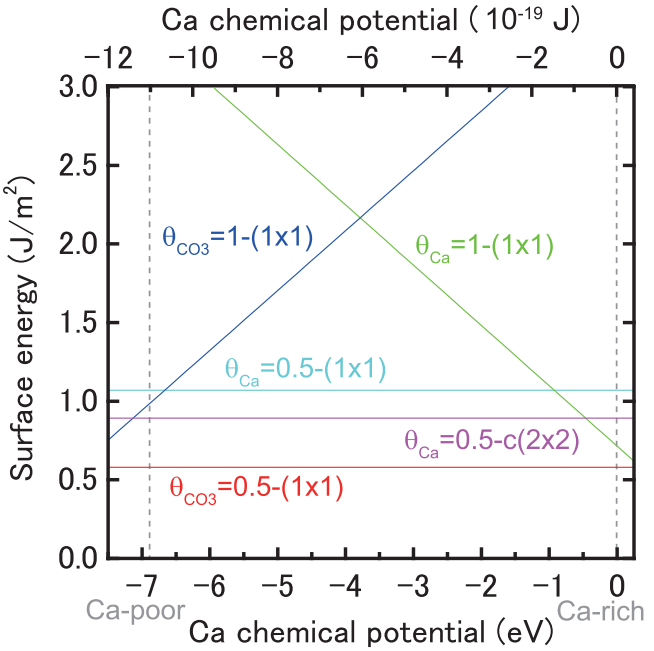

FIG. 7. (Color online) Calculated surface energy E_{surf} (in J/m^2) of aragonite {001} surface as a function of Ca chemical potential μ_{Ca}. The notation is the same as in Fig. 1.

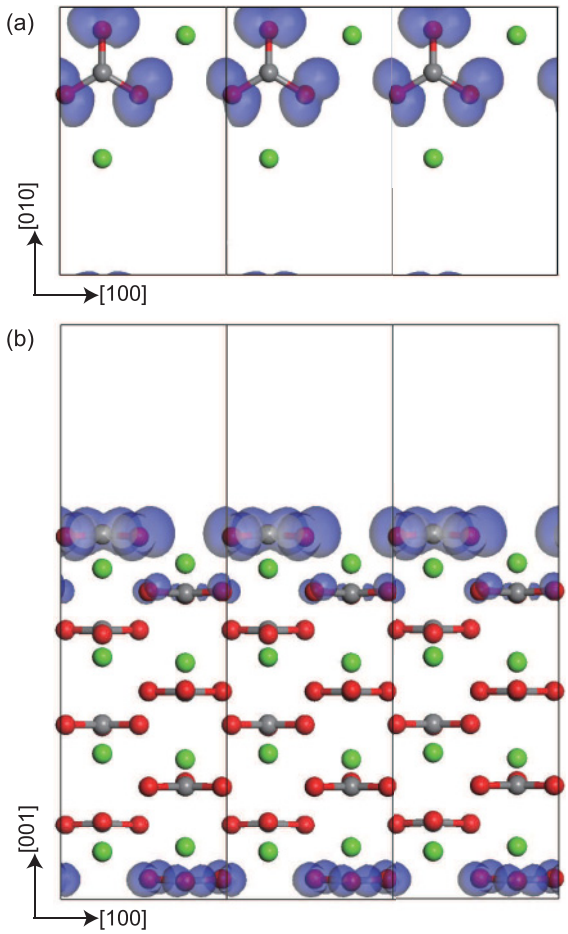

FIG. 8. (Color online) (a) Top and (b) side views of the optimized geometry of the stable aragonite {001}-(1 × 1) surface with $\theta_{CO_3} = 0.5$. The notation is the same as in Fig. 2. Isosurface of squared wave function for the occupied surface state (0.002 electron/Å^3) at Γ point, which is located at 0.6 eV above the valence band maximum of bulk $CaCO_3$, is also shown.

and $\theta_{CO_3} = 1$ have low surface energies under Ca-rich and Ca-poor conditions, respectively. Therefore the {001} plane experimentally observed is considered to be CO_3-terminated surface with $\theta_{CO_3} = 0.5$. It should be noted that the $c(2 \times 2)$ surface with $\theta_{Ca} = 0.5$ is energetically favorable compared to that with the 1 × 1 periodicity. Although these surfaces are metastable over the entire range of Ca chemical potential, two dimensional symmetry of CO_3 at the top layer might be crucial for the stability of aragonite {001} surface.

The calculated geometry after atomic relaxation of the {001} surface with $\theta_{CO_3} = 0.5$ is shown in Fig. 8. There is a negligible change in the atomic configurations near the surface. We find that the spacing between the top and second layers (0.91 Å) is only ∼1% shorter than the spacing along the [001] direction in the bulk aragonite. Accordingly, the energy gain caused by the relaxation (0.13 J/m^2) is much smaller than the surface energy itself. It is thus concluded that the atomic relaxation in the lateral plane is a minor contribution to the stability of {001} surface. Similar to the case of calcite surfaces, the outermost C-O bond lengths in CO_3 groups at the top layer (1.29 Å) are found to be slightly shorter than those in the bulk

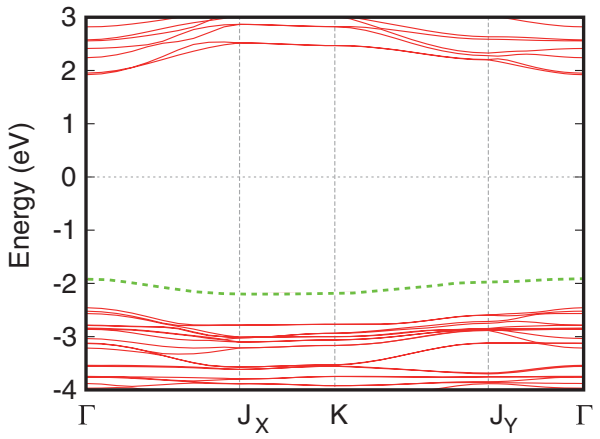

FIG. 9. (Color online) Energy band structures of the stable aragonite {001}-(1 × 1) surface with $\theta_{CO_3} = 0.5$. The notation is the same as in Fig. 3.

region. As a result, there exist surface states leading to the reduction of the C-O bond lengths at the top layer.

Figure 9 shows calculated energy band of the stable {001}-(1 × 1) surface with $\theta_{CO_3} = 0.5$. This energy band clearly shows a character of semiconducting surface, indicating that 4*s* electrons of the Ca atoms located in the second layer are transferred into 2*s* orbitals of the O atoms in CO_3 group at the top layer. The stabilization of the surface with $\theta_{CO_3} = 0.5$ can be interpreted in terms of the electron counting model.[40] Furthermore, we find that the completely occupied surface states emphasized by green (dashed) lines in Fig. 9 are located above the valence band maximum of bulk $CaCO_3$. Our analysis of corresponding Kohn-Sham orbitals shown in Fig. 8 clearly shows that these states possess the character of 2*p* orbitals of O atoms located at the top layer. These surface states are lifted up from corresponding valence bands by ∼0.6 eV since no Ca atoms which are positively charged are coordinated above the top layer. The reduction of outermost C-O bond in CO_3 groups at the top layer can be attributed to these surface states.

D. Aragonite {010} and {110} surfaces

There is a layer unit consisting of four atomic layers along both the [010] and [$\bar{1}$10] directions for aragonite {010} and {110} surfaces, respectively. This layer in the 1 × 1 lateral unit consists of two CO_3 layers each of which are constructed of one CO_3 group, and two Ca layers each of which are of one Ca atom. Therefore in both {010} and {110} orientations there are four distinctive ways of termination of $CaCO_3$ whose coverage are either 0.5 or 1. We obtain similar surface energies with each other on these orientations since the triangular planes of CO_3 groups are aligned normal to the surface in both {010} and {110} surfaces. Figure 10 shows the surface energies of {010} and {110} surfaces as a function of Ca chemical potential. In these orientations, the surfaces satisfying $\theta_{Ca} = 0.5$ have the lowest surface energy for the possible range of Ca chemical potential. The stable atomic configurations on these orientations is different from those on the {001} surface. The surfaces Ca-terminated and CO_3-terminaed surfaces with $\theta_{Ca} = 1$ and $\theta_{CO_3} = 1$ have higher surface energies, indicating

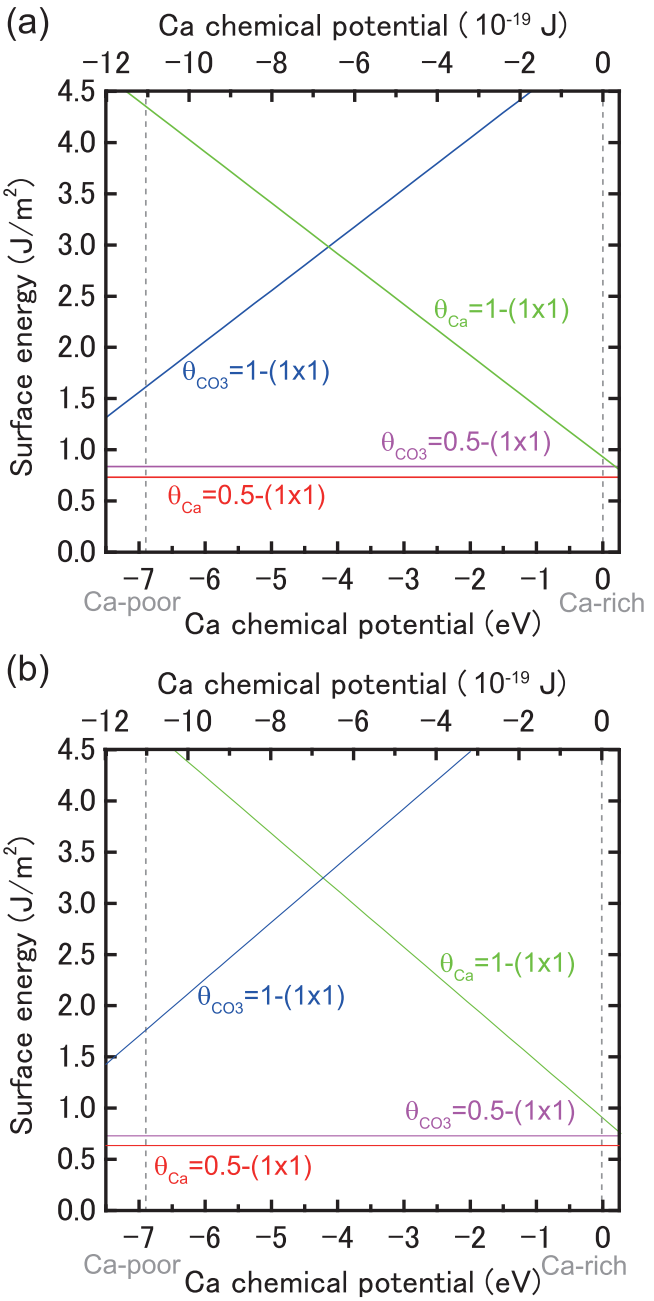

FIG. 10. (Color online) Calculated surface energy E_{surf} (in J/m^2) of aragonite (a) {010} and (b) {110} surface as a function of Ca chemical potential μ_{Ca}. The notation is the same as in Fig. 1.

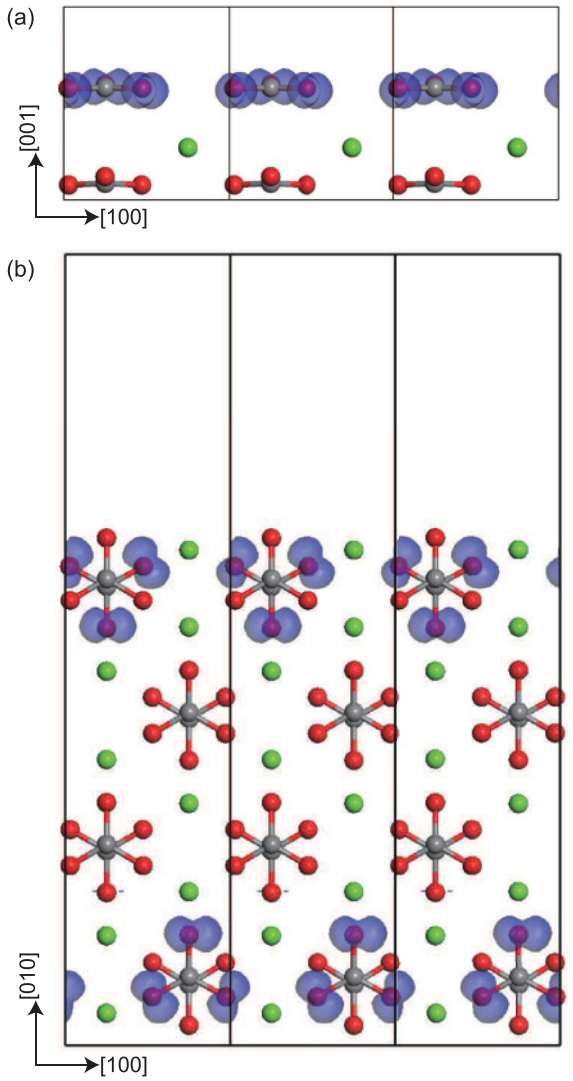

FIG. 11. (Color online) (a) Top and (b) side views of the optimized geometry of the stable aragonite {010} surface with $\theta_{Ca} = 0.5$. The notation is the same as in Fig. 2. Isosurface of squared wave function for the occupied surface state (0.005 electron/Å^3) at Γ point, which is located at 0.3 eV above the valence band maximum of bulk $CaCO_3$, is also shown.

that they are always metastable. It is thus likely that the {010} and {110} surfaces experimentally observed corresponds to the surfaces satisfying $\theta_{Ca} = 0.5$. The calculated energies of these surfaces (0.73 and 0.64 J/m^2 for {010} and {110} surfaces, respectively) are lower than those in the previous calculation (0.96 and 0.88 and J/m^2 for {010} and {110} surfaces,[15] respectively). As mentioned above, the difference between present DFT calculation and the empirical potential calculation might be due to the effect of dipole moments, which are locally formed between Ca^{2+} in the top layer and CO_3^{2-} in the second layer.

The calculated geometries after atomic relaxation of the {010} and {110} surfaces with $\theta_{Ca} = 0.5$ are shown in Figs. 11 and 12, respectively. One of the prominent features of these surfaces different from those of the stable {001} surface is the termination of $CaCO_3$. The top layer of these surfaces in the 1×1 unit is constructed of one Ca atom. In contrast to the {001} surface, we find a contraction of the spacing between the top Ca and the second CO_3 layers. These Ca atoms moves toward bulk region by 0.30–0.31 Å and the spaces are found to be reduced by 30 and 15% compared to those in the bulk phase on {010} and {110} surfaces, respectively. Furthermore, the outermost O atom of CO_3 in the second layer moves along the [001] and [100] directions by 0.15–0.16 Å toward the Ca atom at the top layer on {010} and {110} surfaces, respectively. As a result of these atomic relaxation, the contribution of surface relaxation (∼0.28 J/m^2) on the surface energy in {010} and

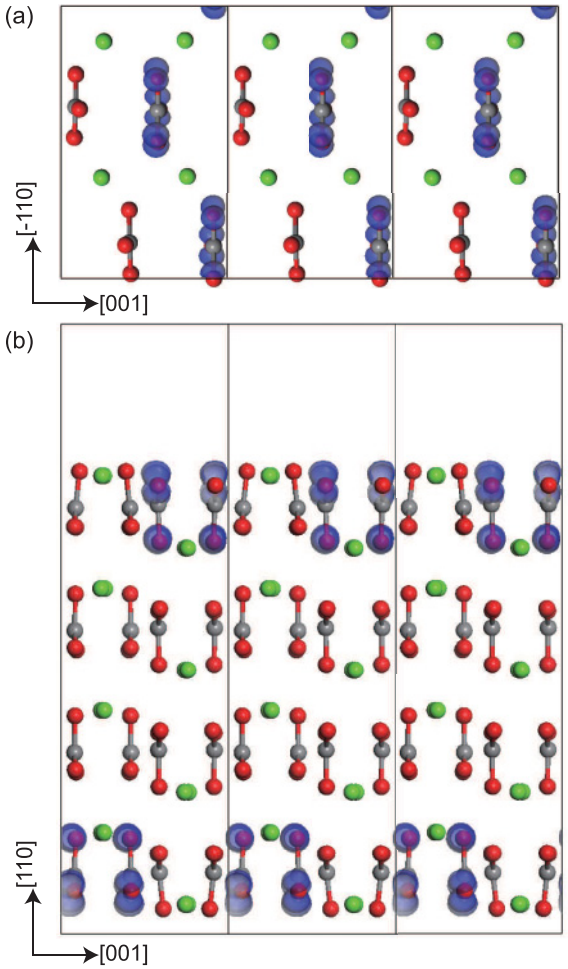

FIG. 12. (Color online) (a) Top and (b) side views of the optimized geometry of the stable aragonite {110} surface with $\theta_{Ca} = 0.5$. The notation is the same as in Fig. 2. Isosurface of squared wave function for the occupied surface state (0.004 electron/Å^3) at Γ point, which is located at 0.2 eV above the valence band maximum of bulk $CaCO_3$, is also shown.

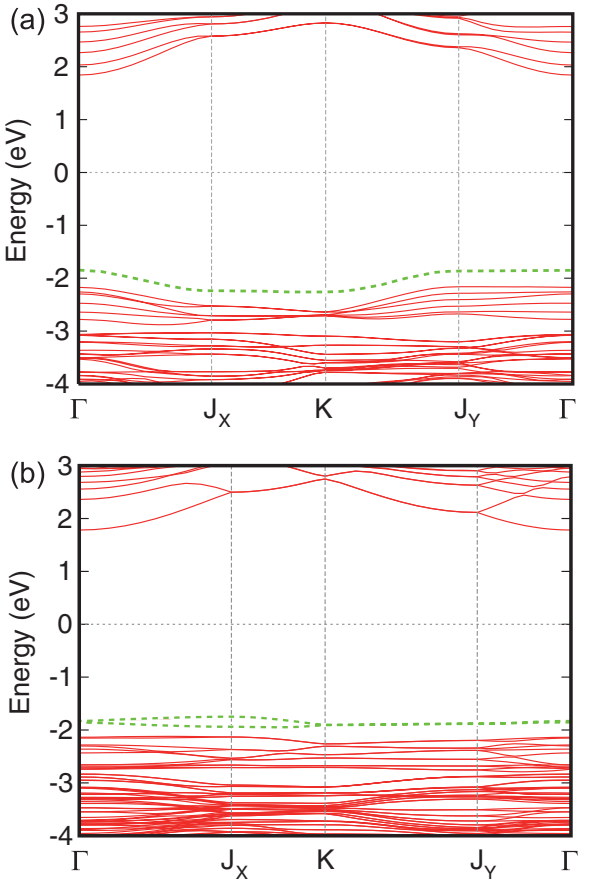

FIG. 13. (Color online) Energy band structures of the stable aragonite (a) {010} and (b) {110} surfaces with $\theta_{Ca} = 0.5$. The notation is the same as in Fig. 3.

{110} surfaces is relatively large compared to that in the {001} surface. It is thus concluded that the atomic relaxation in the lateral plane play a role on the stability of these surfaces. Even though outermost CO_3 groups are located in the second layer, the outermost C-O bond lengths in these CO_3 groups (1.29 and 1.27 Å for {010} and {110} surfaces, respectively) are still shorter than those in bulk aragonite. This implies the appearance of surface states which cause the difference in the C-O bond lengths at the second layer.

Similarity in the energy band between the {010} and {110} surfaces can also be recognized, as shown in Fig. 13. The energy bands of these surfaces clearly show a character of semiconducting surface. This is originating from the transfer of electrons between 4*s* electrons of the Ca atoms at the top layer and 2*s* orbitals of the O atoms in CO_3 group located at the second layer. The stabilization of the surface with $\theta_{Ca} = 0.5$ can be interpreted in terms of the electron counting model.[40] We also find that the completely occupied surface states emphasized by green (dashed) lines in Figs. 13(a) and 13(b) for the {010} and {110} surfaces, respectively, are located above the valence band maximum of bulk $CaCO_3$. Similar to the case of {001} surface, these states possess the character of 2*p* orbitals of O atoms located at the second layer as shown in Figs. 11 and 12 for {010} and {110} surfaces, respectively. These surface states are lifted up from corresponding valence bands by ∼0.3 and ∼0.2 eV for {010} and {110} surfaces, respectively. The energy shift are smaller than that on {001} surface since negatively charged CO_3 groups are coordinated in the second layer. However, less Ca atoms which are positively charged still exist above the second layer. Owing to this atomic configuration, these surface states are lifted up from corresponding valence bands, leading to the reduction of outermost C-O bond in CO_3 groups in the second layer.

E. Surface energies

Table II summarizes the calculated surface energies of the stable surfaces for various orientations, along with those obtained by previous calculations. Since these surfaces maintain the stoichiometry of bulk $CaCO_3$, their surface energies are irrespective of the chemical potential of constituting elements. The stability of these surfaces is thus determined in terms of the surface energy over the wide range of crystal growth conditions. For calcite surfaces, the $\{10\bar{1}4\}$ surface with $\theta_{Ca} = \theta_{CO_3} = 1$ has the lowest surface energy, and its surface energy (0.51 J/m^2) is much lower than the other one by

TABLE II. Calculated surface energy E_{surf} of the stable $CaCO_3$ surfaces for various orientations, along with those in the previous empirical potential and density-functional theory (DFT) calculations.[15–21]

Polymorph	Orientation	$\theta_{Ca}/\theta_{CO_3}$	E_{surf} (J/m^2)	Authors	Calculation method
calcite	$\{10\bar{1}4\}$	$\theta_{Ca} = \theta_{CO_3} = 1$	0.51	This work	DFT
			0.59	de Leeuw and Parker[a]	empirical potential
			0.57	Nygren *et al.*[b]	empirical potential
			0.60	Duffy and Harding[c]	empirical potential
			0.53	Rohl *et al.*[d]	empirical potential
			0.42	Parker *et al.*[e]	DFT
			0.50	Bruno *et al.*[f]	DFT
	$\{01\bar{1}2\}$	$\theta_{Ca} = 0.5$	0.89	This work	DFT
			1.25	Duffy and Harding[c]	empirical potential
			1.06	Bruno *et al.*[f]	DFT
	$\{01\bar{1}2\}$	$\theta_{CO_3} = 0.5$	0.72	This work	
			1.06	Duffy and Harding[c]	empirical potential
			0.75	Bruno *et al.*[f]	DFT
aragonite	{001}	$\theta_{Ca} = 0.5$	0.89	This work	DFT
			1.05	de Leeuw and Parker[a]	empirical potential
	{001}	$\theta_{CO_3} = 0.5$	0.58	This work	DFT
			0.85	de Leeuw and Parker[a]	empirical potential
	{010}	$\theta_{Ca} = 0.5$	0.73	This work	DFT
			0.96	de Leeuw and Parker[a]	empirical potential
	{010}	$\theta_{CO_3} = 0.5$	0.84	This work	DFT
			1.50	de Leeuw and Parker[a]	empirical potential
	{110}	$\theta_{Ca} = 0.5$	0.64	This work	DFT
			0.88	de Leeuw and Parker[a]	empirical potential
	{110}	$\theta_{CO_3} = 0.5$	0.73	This work	DFT
			1.04	de Leeuw and Parker[a]	empirical potential

[a]Reference 15.
[b]Reference 16.
[c]Reference 17.
[d]Reference 18.
[e]Reference 19.
[f]Reference 20.

more than 0.21 J/m^2. This implies that the $\{10\bar{1}4\}$ surface is the most stable surface among various orientations and is dominant during the growth and equilibrium morphology of calcite crystal. The stability of calcite surfaces is thus consistent with the experimental findings.[2] Among various orientations in aragonite surfaces, the {001} surface with $\theta_{CO_3} = 0.5$ has the lowest surface energy. The the {110} surface with $\theta_{Ca} = 0.5$ has low surface energy (0.64 J/m^2) close to that of the {001} surface with $\theta_{CO_3} = 0.5$. Therefore it is likely that these surfaces are stable and dominant in the experimental morphology of aragonite crystal. Actually, the plausibility of the stable {001} surface obtained from our calculations is consistent with the observation of {001} surface under biogenic environments,[14] and that of some planes whose angle and positions could be assigned to the {001} surface.[23] The stability of {110} surface is also consistent with the emergence of {110} orientation in the experimental morphology of aragonite crystal.[22]

IV. SUMMARY

We have investigated the structural stability and electronic structure of $CaCO_3$ surfaces in calcite and aragonite polymorphs using the electronic structure calculations within the density-functional theory. Each plane has several distinctive surface terminations. We have performed systematic calculations to reveal surface atomic relaxation, surface energies, and electronic structures. We have found that in both calcite and aragonite surfaces the surfaces with the same number of Ca atoms as $CaCO_3$ groups have the lowest surface energy over the wide range of Ca chemical potential. Detailed atomic structures of each surface has been obtained, which is imperative for atom-scale clarification of reaction of the surfaces. The electronic states of each plane have been calculated in detail. The surface states located above the valence band maximum result in the reduction of C-O bonds in carbonate groups at the top or second layer, and offer a possibility to identify the atomic structures by spectroscopic measurements. The determination of atomic arrangements, along with the corresponding surface electronic states, has been interpreted in terms of their ionicity, metalicity, and covalency. This would give several insights to atom-scale quantitative identification and characterization of $CaCO_3$ surfaces, and provide a firm theoretical framework to consider atomically controlled growth and deposition of important materials on $CaCO_3$.

ACKNOWLEDGMENT

This work was supported in part by a Grant-in-Aid for Scientific Research from JSPS under Contract No. 21560032. Codes used in this work are based on Tokyo *ab initio* program package (TAPP), which has been developed by a consortium initiated at The University of Tokyo. Computations were performed at RCCS (National Institutes of Natural Sciences).

*akiyama@phen.mie-u.ac.jp

[1] N.-S. Park, M.-W. Kim, S. C. Langford, and J. T. Dickinson, J. Appl. Phys. **80**, 2680 (1996).
[2] P. M. Dove and M. F. Hochella Jr., Geochim. Cosmochim. Acta **57**, 705 (1993).
[3] D. Chakraborty and S. K. Bhatia, Ind. Eng. Chem. Res. **35**, 1995 (1996).
[4] B. R. Heywood and S. Mann, Chem. Mater. **6**, 311 (1994).
[5] S. L. Stipp, W. Gutmannsbauer, and T. Lehmann, Amer. Mineral. **81**, 1 (1996).
[6] F. Ohnesorge and G. Binnig, Science **260**, 1451 (1993).
[7] S. L. S. Stipp, C. M. Eggleston, and B. S. Nielsen, Geochim. Cosmochim. Acta **58**, 3023 (1994).
[8] Y. Liang, A. S. Lea, D. R. Baer, and M. H. Engelhard, Surf. Sci. **351**, 172 (1996).
[9] S. Rode, N. Oyabu, K. Kobayashi, H. Yamada, and A. Kühnle, Langmuir **25**, 2850 (2009).
[10] Y. Qian, N. Sturchio, R. Chiarello, P. Lyman, T. Lee, and M. Bedzyk, Science **265**, 1555 (1994).
[11] U. Magdans, H. Gies, X. Torrelles, and J. Rius, Eur. J. Mineral. **18**, 83 (2006).
[12] S. L. Stipp and M. F. Hochella, Geochim. Cosmochim. Acta **55**, 1723 (1991).
[13] M. E. Marsh and R. L. Sass, Science **208**, 1262 (1980).
[14] W. T. Hou and Q. L. Feng, J. Cryst. Growth **258**, 402 (2003).
[15] N. H. de Leeuw and S. C. Parker, J. Phys. Chem. B **102**, 2914 (1998).
[16] M. A. Nygren, D. H. Gay, C. R. A. Catlow, M. P. Wilson, and A. L. Rohl, J. Chem. Soc. Faraday Trans. **94**, 3685 (1998).
[17] D. M. Duffy and J. H. Harding, J. Mater. Chem. **12**, 3419 (2002).
[18] A. L. Rohl, K. Wright, and J. D. Gale, Amer. Mineral. **88**, 921 (2003).
[19] S. C. Parker, S. Kerisit, A. Marmier, S. Grigoleit, and G. W. Watson, Faraday Discuss. **124**, 155 (2003).
[20] M. Bruno, F. R. Massaro, M. Prencipe, and D. Aquilano, CrystEngComm **12**, 3626 (2010).
[21] M. Bruno, F. R. Massaro, and M. Prencipe, Surf. Sci. **602**, 2774 (2008).
[22] E. S. Dana, *A Textbook of Mineralogy* (Wiley, New York, 1958).
[23] W. A. Deer, R. A. Howie, and J. Zussman, *Introduction to the Rock Forming Minerals* (Longman, Harlow, 1992).
[24] P. Hohenberg and W. Kohn, Phys. Rev. **136**, B864 (1964).
[25] W. Kohn and L. J. Sham, Phys. Rev. **140**, A1133 (1965).
[26] J. P. Perdew, K. Burke, and M. Ernzerhof, Phys. Rev. Lett. **77**, 3865 (1996).
[27] D. Vanderbilt, Phys. Rev. B **41**, 7892 (1990).
[28] J. Yamauchi, M. Tsukada, S. Watanabe, and O. Sugino, Phys. Rev. B **54**, 5586 (1996).
[29] H. Kageshima and K. Shiraishi, Phys. Rev. B **56**, 14985 (1997).
[30] M. Tsukada *et al.*, Computer program package TAPP, University of Tokyo, Tokyo, Japan, 1983–2011.
[31] E. N. Maslen, V. A. Streltsov, and N. R. Streltsova, Acta Crystallogr. Sect. B **49**, 636 (1993).
[32] D. R. Baer and D. L. Balnchard, Appl. Surf. Sci. **72**, 295 (1993).
[33] J. Balmain, B. Hannoyer, and E. Lopez, J. Biomed. Mater. Res. **48**, 749 (1999).
[34] A. J. Skinner, J. P. La Femina, and H. J. F. Jansen, Amer. Mineral. **79**, 205 (1994).
[35] S. K. Medeiros, E. L. Albuquerque, F. F. Maia Jr., E. W. S. Caetano, and V. N. Freire, J. Phys. D **41**, 065405 (2008).
[36] F. M. Hossain, G. E. Murch, I. V. Belova, and B. D. Turner, Solid State Commun. **149**, 1201 (2009).
[37] M. Prencipe, F. Pascale, C. M. Zicovich-Wilson, V. R. Saunders, R. Orlando, and R. Dovesi, Phys. Chem. Miner. **31**, 559 (2004).
[38] S. K. Medeiros, E. L. Albuquerque, F. F. Maia Jr., E. W. S. Caetano, and V. N. Freire, Chem. Phys. Lett. **430**, 293 (2006).
[39] The convergence of the surface energy with respect to the thicknesses of the slab and the vacuum region is examined by the calculations of calcite $\{10\bar{1}4\}$ and aragonite {001} surfaces consisting of seven bilayers and six trila yers of $CaCO_3$ with the ∼13 Å vacuum region, respectively. The values of surface energy vary by only 0.04 J/m^2 (3 meV/Å^2) depending on the thicknesses of the slab and the vacuum region, and the energy difference between unequivalent structures are converged within 0.008 J/m^2 (0.5 meV/Å^2). It is thus concluded that the error caused by the slab model is negligible and the stability of $CaCO_3$ surfaces is definitely obtained in the present models.
[40] M. D. Pashley, K. W. Haberern, W. Friday, J. M. Woodall, and P. D. Kirchner, Phys. Rev. Lett. **60**, 2176 (1988).
[41] Recent experimental and theoretical studies have found a high-pressure polymorph called postaragonite phase with space group P_{mmm} (see, A. R. Oganov, C. W. Glass, and S. Ono, Earth Planet. Sci. Lett. **241**, 95 (2006)). This polymorph is not taken into account because we here focus on the surfaces under low-pressure conditions.